processes

Article

A Numerical Study on the Performance of the H_2 Shaft Furnace with Dual-Row Top Gas Recycling

Shan Yu [1], Lei Shao [2], Zongshu Zou [2] and Henrik Saxén [3,*]

[1] School of Metallurgy Engineering, Liaoning Institute of Science and Technology, Benxi 117004, China; windhat@163.com
[2] School of Metallurgy, Northeastern University, Shenyang 110819, China; shaolei@mail.neu.edu.cn (L.S.); zouzs@mail.neu.edu.cn (Z.Z.)
[3] Process and Systems Engineering Laboratory, Åbo Akademi University, FI-20500 Åbo, Finland
* Correspondence: hsaxen@abo.fi; Tel.: +358-40-5443301

Abstract: Given the urgent pursuit of carbon neutrality and stringent climate policies, the H_2 shaft furnace (H_2-SF) is starting to gain widespread attention in the steel industry. In this study, the performance of the H_2-SF under operation with a dual-row injection top gas recycling system was investigated by a one-dimensional mathematical model. The potential of microwave heating as a means to supply thermal energy in regions of energy deficit was also assessed briefly. The results showed that for scenarios without microwave heating, increasing the upper-row injection rate can improve the furnace performance, and increasing the distance of the upper-row injection level from the furnace top also has a positive effect. A high microwave heating efficiency is expected in regions above the upper-row injection level. For scenarios with microwave heating, a higher microwave power leads to a better furnace performance. Thus, a higher furnace productivity can be achieved by increasing either the upper-row injection rate or the microwave power. However, the latter seems more promising as it decreases the total energy demand due to a better utilization of thermal energy. Based on the comparison of two representative examples, the decrease in the total energy demand is about 0.2 GJ/t-Fe.

Keywords: H_2 shaft furnace; energy demand; dual-row injection; microwave heating; sustainable steelmaking

check for updates

Citation: Yu, S.; Shao, L.; Zou, Z.; Saxén, H. A Numerical Study on the Performance of the H_2 Shaft Furnace with Dual-Row Top Gas Recycling. *Processes* **2021**, *9*, 2134. https://doi.org/10.3390/pr9122134

Academic Editor: Haiping Zhu

Received: 24 October 2021
Accepted: 23 November 2021
Published: 26 November 2021

1. Introduction

Steel is undisputedly a central material component for modern societies, and its global demand is forecast to reach 2500 million tons in 2050 [1], mainly driven by population growth together with infrastructure construction/improvement in developing countries. At present, the dominant steelmaking route involves the coal-based blast furnace, where coke is used as a fundamental raw material for providing the reduction potential, permeability for the gas flow in the upper part of the furnace and liquid flow in the lower part, as well as carbon for the hot metal. Consequently, steelmaking today has a specific emission of approximately 1.9 t-CO_2/t-steel and accounts for 7% of the global anthropogenic CO_2 emissions [2]. Given the urgent pursuit of carbon neutrality and stringent climate policies, the steel industry must significantly reduce its carbon footprint via adopting novel sustainable steelmaking technologies. Under these circumstances, hydrogen (H_2) has gained rapidly rising popularity [3–5] as a reductant of iron ore with no other emissions than water vapor (H_2O). Several pilot projects of H_2-based steelmaking are currently underway, such as HYBRIT in Sweden [6] and μDRAL in Germany [7].

In essence, the H_2-based steelmaking chain runs on electricity and mainly consists of three sub-processes: H_2 reduction (for converting iron oxide pellets to direct reduced iron, DRI), electric heating (for melting DRI and steelmaking) and water electrolysis (for generating H_2). These are in practice realized using a direct reduction shaft furnace operated with pure H_2 (H_2-SF), an electric arc furnace (EAF) as well as a (large-scale) electrolyzer, respectively. By utilizing clean (e.g., wind, solar or even nuclear) energy-based electricity, the specific emission of this new steelmaking route may be reduced to 0.05 t-CO_2/t-steel [8], with emissions mainly from the injection of carbon for refinement of liquid steel and the inevitable consumption of graphite electrodes in the EAF. In light of its substantial emissions-reduction potential, the H_2-based steelmaking route is starting to gain worldwide acceptance, simultaneously leading to pioneering studies mostly focused on key issues including (1) assessment of the process economics and (2) understanding and then improvement of the H_2-SF performance.

The first issue is of unequivocal importance since the production cost determines whether the process is commercially competitive, even though an extensive access to clean energy is foreseeable in the future. Vogl et al. [8] were among the first who assessed the H_2-based steelmaking route in terms of energy demand and production cost. It was reported that the entire process needs 3.48 MWh of electricity to produce one ton of liquid steel, and the total production cost is highly sensitive to the price of electricity. The H_2-based route becomes economically viable only if electricity costs less than 20 EUR/MWh. When the CO_2 emission tax is higher than 62 EUR/t-CO_2, however, the new route tends to be competitive with the conventional blast furnace (basic oxygen furnace) route at an electricity price of less than 40 EUR/MWh. It is interesting to note that the present CO_2 emission tax in the European Union is approaching the mentioned threshold value, but the electricity price is far higher than 40 EUR/MWh. As for the second issue regarding H_2-SF performance, due attention is required since the use of pure H_2 introduces new challenges owing to the endothermic nature of H_2 reduction of iron oxides. In principle, utilization of chemical energy of the gas in the H_2-SF is poor since an excessively large amount of H_2 is needed as a carrier of thermal energy ("sensible heat") in order to meet the considerable heat demand of the endothermic reactions and heating of the burden in the furnace. Ranzani da Costa et al. [9] built a mathematical model based on a description of the local mass, energy and momentum balances for the gas and solid species in a H_2-SF. The simulation results showed that complete conversion of the (100% hematite) pellets to metallic iron (i.e., a DRI metallization degree of 1.0) is obtained in the furnace if a preheated H_2 (98%) + H_2O (2%) gas stream of 1073 K is injected at a specific flow rate of 1609 Nm^3/t-pellet. It can be further calculated that the top gas utilization degree (i.e., mole fraction of H_2O in the gas mixture consisting of H_2O and H_2) is roughly 0.27 under the operating conditions considered. The present authors [10] also developed a H_2-SF model and predicted that the top gas utilization degree is generally lower than 0.25 for scenarios where pure H_2 is injected into the furnace and the target DRI metallization degree is (close to) 1.0. In a recent publication [11], the study was extended to a new top gas recycling (TGR) concept featuring dual-row injection as an alternative way of relaxing the strong constraints imposed by the need to supply a large portion of thermal energy to the process. This preliminary assessment confirmed that the dual-row injection TGR system could improve the furnace performance, especially in terms of gas utilization degree and total energy demand. Recently, the state-of-the-art technology of microwave heating that has attracted widespread attention in the field of pyro-metallurgy [12,13] has appeared as an option of supplying thermal energy to the H_2-SF. However, there is so far very little information on the use of microwave heating in shaft furnaces.

With the above motivations, the current work aims to clarify whether a better H_2-SF performance can be achieved using a combination of the dual-row injection TGR system and microwave heating technology. For this, a thorough numerical study was first carried out to determine a proper level of the upper-row injection, above which a microwave heater is installed. After studying this, the potential of microwave heating was assessed preliminarily by investigating the effects of microwave power. The findings of this work may serve as guidelines for future design of the H_2-SF as well as for carrying out optimization of existing syngas-based units.

2. Modeling

2.1. H_2-SF Process

Figure 1 schematically depicts the H_2-SF with a microwave heater and configuration of the dual-row injection TGR system. As can be seen, the off-gas from the furnace top is passed through a dry deduster (i.e., A in Figure 1) followed by a (counter-flow) heat exchanger (B), into which a stream of (room-temperature) fresh H_2 generated by an electrolyzer (H) is simultaneously introduced. Thus, the off-gas is dedusted and cooled, while the fresh H_2 is preheated. By using a distributor (C), the former gas stream is split into two streams, one of which is compressed in a compressor (F2), heated in a heater (G2) and finally injected into the furnace at a higher (i.e., upper-row injection) level, while the other stream is introduced into a condenser (D) for removing H_2O to recover the remaining H_2. The recovered H_2 is then blown into a mixer (E), together with the preheated fresh H_2 from the heat exchanger (B). After mixing, the gas is compressed (F1), heated (G1) and finally injected into the furnace at a lower-row injection level. In addition, a microwave heater (*J*) with a height of *U* is installed above the upper-row injection, as also depicted in Figure 1.

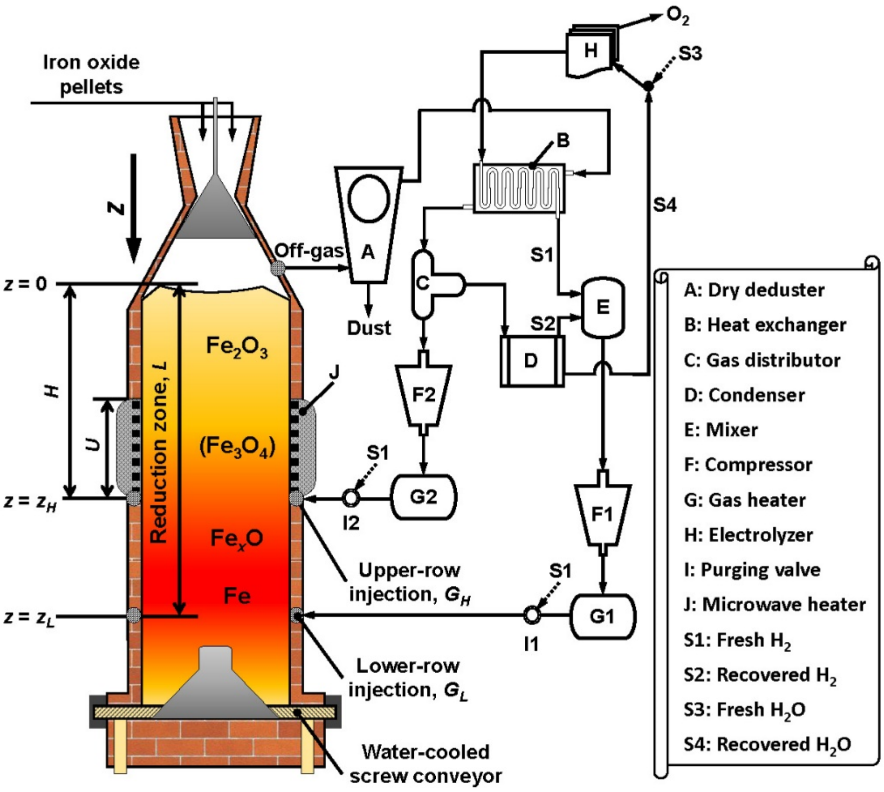

Figure 1. Schematic of the H_2-SF with a microwave heater and configuration of the dual-row injection TGR system.

2.2. H_2-SF Model

The H_2-SF model is similar to the one employed in the previous work where the potential of the dual-row injection TGR system was assessed, except for some extensions made to incorporate the effects of microwave heating. For the sake of simplification, the energy that the solid phase can effectively absorb under microwave heating is considered to decrease with the mass fraction of metallic iron in the solid. This is motivated by the fact that metals reflect microwaves and cannot be heated efficiently. In the following, only the key treatment and governing equations of the model are outlined: the reader is referred to Shao et al. [10] for detailed information about it.

The mathematical model was built based on a description of the complex gas–solid countercurrent reactive flow in the reduction zone of the furnace (cf. Figure 1). The gas phase consists of five species: CO, H_2, CO_2, H_2O and N_2, and the solid phase contains Fe_2O_3, Fe_3O_4, wustite (Fe_xO, $x = 0.95$), Fe as well as inert gangue components (being mainly CaO, SiO_2, MgO and Al_2O_3). At a temperature above 849 K, the solid iron oxides are reduced by CO and H_2 following three consecutive steps: $Fe_2O_3 \rightarrow Fe_3O_4$, $Fe_3O_4 \rightarrow Fe_xO$ and $Fe_xO \rightarrow Fe$. When the temperature is below 849 K, the reduction occurs in two consecutive steps: $Fe_2O_3 \rightarrow Fe_3O_4$ and $Fe_3O_4 \rightarrow Fe$, since Fe_xO is unstable at low temperatures. It is obvious that the model can be used to simulate the operation of H_2-SF by simply setting the contents of CO, CO_2 and N_2 in the feed gas equal to zero.

Algebraic manipulation of the local mass, energy and momentum balances of the gas and solid phases gives rise to a set of coupled nonlinear ordinary differential equations (ODEs) for the gas temperature (T_g), mole fraction of gaseous species (Y_i, $i = 1, \ldots, 4$ representing H_2, CO, H_2O and CO_2), solid temperature (T_s), reduction degree of the reduction steps (X_j, $j = 1, \ldots, 4$ denoting reduction steps $Fe_2O_3 \rightarrow Fe_3O_4$, $Fe_3O_4 \rightarrow Fe_xO$, $Fe_xO \rightarrow Fe$ and $Fe_3O_4 \rightarrow Fe$) as well as gas pressure (P_g).

The gas temperature is given by:

$$\frac{dT_g}{dz} = \frac{6(1-\varepsilon)}{d_p}\frac{S}{\rho_g G}\frac{h_p}{C_g}\left(T_g - T_s\right) + \frac{\pi D}{\rho_g G}\frac{h_w}{C_g}\left(T_g - T_a\right) \tag{1}$$

where z is the vertical downward direction (cf. Figure 1). The variables ε, d_p, S, ρ_g, G, C_g, D, h_p, h_w and T_a are the bed porosity, pellet diameter, cross-sectional area of the reduction zone, density of gas, volumetric flow rate of gas, specific heat capacity at constant pressure, inner diameter of the reduction zone, gas–solid heat transfer coefficient, overall heat transfer coefficient over the furnace wall as well as ambient temperature, respectively.

The mole fractions of the gas species are obtained from:

$$\frac{dY_i}{dz} = \frac{6(1-\varepsilon)}{\pi d_p^3}\frac{S}{n_g}\sum_{j=1}^{4}\alpha V_{i,j}, \begin{cases} \alpha = 1, \text{ if } i \le 2 \\ \alpha = -1, \text{ if } i > 2 \end{cases} \tag{2}$$

where n_g and V are the molar flow rate of gas and the reduction rate of a single pellet.

In the above equation, V is computed using the widely accepted multi-step unreacted shrinking core model (see Hara et al. [14] for a thorough description).

The burden temperature is given by:

$$\frac{dT_s}{dz} = \frac{6(1-\varepsilon)}{d_p}\frac{S}{W}\frac{h_p}{C_s}\left(T_g - T_s\right) - \frac{6(1-\varepsilon)}{\pi d_p^3}\frac{S}{W}\frac{1}{C_s}\sum_{i=1}^{2}\sum_{j=1}^{4}V_{i,j}\Delta H_{i,j} - \frac{S}{W}\frac{\varepsilon}{C_s}V_{wg}\Delta H_{wg} + \frac{\lambda(1-\omega_{Fe})}{U}\frac{S}{W}\frac{1}{C_s}E_{mw} \tag{3}$$

where W, C_s, ΔH, V_{wg} and ΔH_{wg} are the mass flow rate of solid, specific heat capacity of solid, reaction enthalpy of each reduction step, reaction rate and enthalpy of the water gas shift reaction, respectively. The rightmost term in the equation represents the energy that the solid phase absorbs by microwave heating. The variables λ, ω_{Fe} and E_{mw} are the efficiency factor of the heater, mass fraction of metallic iron in the solid phase and power of the microwave heater, respectively. It should be noted that E_{mw} is nonzero only in the region covered by the microwave heater.

The reduction degrees of the iron oxides are given by:

$$\frac{dX_j}{dz} = \frac{6(1-\varepsilon)}{\pi d_p^3}\frac{S}{W\beta_j\kappa}\sum_{i=1}^{2}V_{i,j} \tag{4}$$

where β and κ are the initial oxygen mole fraction of each iron oxide and the total reducible oxygen content of the initial pellet.

Finally, the gas pressure is given by:

$$\frac{dP_g}{dz} = 150\frac{(1-\varepsilon)^2}{\varepsilon^3}\frac{\mu_g u_g}{d_p^2} + 1.75\frac{(1-\varepsilon)}{\varepsilon^3}\frac{\rho_g u_g^2}{d_p} \tag{5}$$

where μ_g and u_g are the dynamic viscosity and superficial velocity of the gas.

For the two-point boundary conditions that result from the nature of the countercurrent flows, the solution of the ODEs can be found by a shooting method. For detailed information about the numerical method, the reader is referred to Shao et al. [10]. The total energy demand of the entire process is the sum of the energy demand of electrolysis, compression and heating. In the computation of the last term, the recycled heat for preheating the fresh H_2 in the counter-flow heat exchanger is subtracted. The reader is referred to Karwa [15] for the effectiveness NTU (number of transfer units) method, which is used to estimate the recycled heat in the counter-flow heat exchanger (cf. B in Figure 1).

2.3. Model Parameters

The main parameters used in the model are provided in this section. Table 1 presents the correlations used for the chemical reaction rate constants and effective diffusion coefficients concerning H_2 reduction of the pellets considered in the model [16]. Table 2 presents the geometry parameters and the boundary conditions of the model, while Table 3 reports parameters needed for the evaluation of the energy demand of the system.

Table 1. Correlations [16] of chemical reaction rate constant (k) and effective diffusion coefficient (D_{eff}) concerning H_2 reduction of the pellets considered in the model.

Reduction Step	**Correlation for k, cm/s**	**Correlation for D_{eff}, cm^2/s**
$Fe_2O_3 \to Fe_3O_4$ or $Fe_3O_4 \to Fe$	$\exp\left(4.49 - \frac{33.4}{RT_s}\right)$	$\exp\left(3.43 - \frac{4.2\times10^3}{T_s}\right)$
$Fe_3O_4 \to Fe_xO$	$\exp\left(6.70 - \frac{58.2}{RT_s}\right)$	$\exp\left(5.64 - \frac{6.8\times10^3}{T_s}\right)$
$Fe_xO \to Fe$	$\exp\left(6.97 - \frac{57.1}{RT_s}\right)$	$\exp\left(4.77 - \frac{5.9\times10^3}{T_s}\right)$

Table 2. Key specifications and model parameters of the H_2-SF in this work.

Parameter (Symbol)	**Value**	**Parameter (Symbol)**	**Value**
Length of reduction zone (L)	5.0 m	Pellet composition (T.Fe, FeO, CaO, SiO_2, MgO, Al_2O_3, Rest)	64.60, 0.26, 0.26, 3.71, 0.14, 2.18, 1.45 wt.%
Diameter of reduction zone (D)	3.5 m		
Pellet diameter (d_p) and bed porosity (ε)	14.0 mm, 0.4	Top gas pressure ($P_{g,0}$)	1.5 bar
Solid feed rate (W_0)	100 t/h	Gas feed temperature ($T_{g,L}$ and $T_{g,H}$)	1173 K
Solid feed temperature ($T_{s,0}$)	298 K	Lower-row injection rate (G_L)	1200 Nm^3/t-pellet
Initial reduction degree of solid ($X_{\mathrm{total},0}$)	0	Lower-row gas composition (H_2, H_2O)	100.0 vol.%

Table 3. Parameters for assessment of the energy demand.

Parameter	**Value**
Energy demand of electrolyzer	4.9 kWh/Nm^3-H_2
Efficiency factor of compressor	0.7
Efficiency factor of gas heater	0.7
Efficiency factor of microwave heater	0.7
NTU of heat exchanger	5.0
Outlet temperature of condenser	343 K

2.4. Model Validation

In earlier work by the authors [10], the model was validated by comparing its predictions with measured data from a small-scale syngas-based shaft furnace [17,18], showing a reasonable overall agreement. To further assess the accuracy of the model, industrial production data of a MIDREX shaft furnace (Gilmore plant) reported by Parisi and Laborde [19], and later by Shams and Moazeni [20], were used. The reported length and inner diameter of the reduction zone of the industrial furnace are 9.75 and 4.26 m respectively, and the (volumetric) flow rate of the feed gas is 53,863 Nm^3/h. The temperature and species mole fractions of the feed gas are 1203 K and 52.58% H_2, 29.97% CO, 4.65% H_2O, 4.8% CO_2 and 8.1% CH_4 + N_2, respectively. For the sake of simplicity, however, the CH_4 was neglected here and the mole fraction of N_2 was set equal to 8.1% in the simulation presented in this section. In addition, the DRI production rate is 26.4 t/h, with an average metallization degree of 0.93. According to Shams and Moazeni [20], the required solid feed rate is about 37.3 t/h, assuming that the pellets contain 95% Fe_2O_3 and 5% gangue. Thus, the specific gas feed rate can be estimated to be 1444 Nm^3/t-pellet. For other information about the industrial shaft furnace, the reader is referred to Parisi and Laborde [19] and Shams and Moazeni [20].

Figure 2 compares the mole fractions of gaseous species in the top gas as well as the DRI metallization degree reported by the authors with the corresponding values predicted by the model of the present work. As seen in the figure, the model can accurately predict the production data.

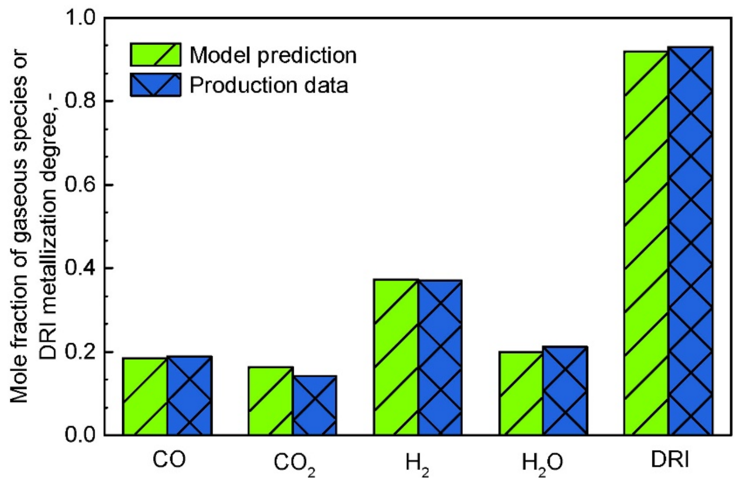

Figure 2. Comparisons between model prediction and industrial production data related to gaseous species in the top gas [19].

3. Results and Discussion

3.1. Effect of Upper-Row Injection Level

Numerical simulations were first conducted to elucidate the H_2-SF performance for different distances (H) of the upper-row injection level from the furnace top (i.e., from the level of z = 0 m, cf. Figure 1) and different injection rates (G_H) with the intent to determine a proper injection level above which the microwave heater should be installed.

As revealed in Figures 3 and 4, an increase in G_H yields an increase in both top gas utilization degree and DRI metallization degree. The underlying reason is that a higher G_H increases the supply of sensible heat to the furnace without deteriorating the in-furnace thermochemical state, since the reduction potential of the gas injected at the upper row is sufficient.

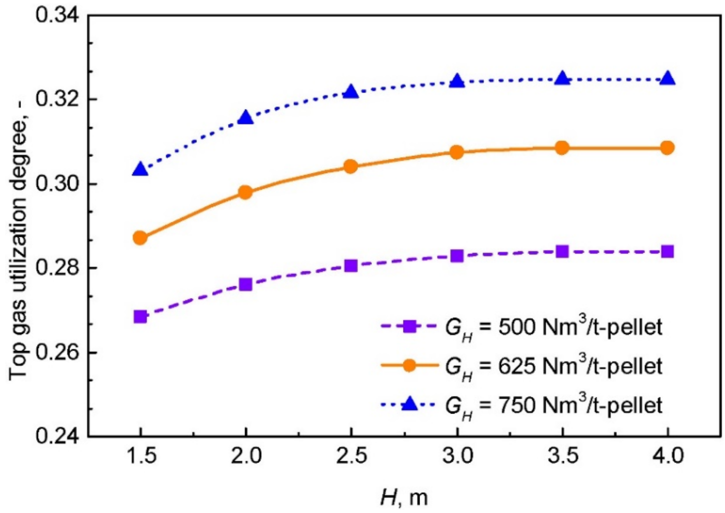

Figure 3. Effect of upper-row injection distance (H) on top gas utilization degree at different injection rates (G_H).

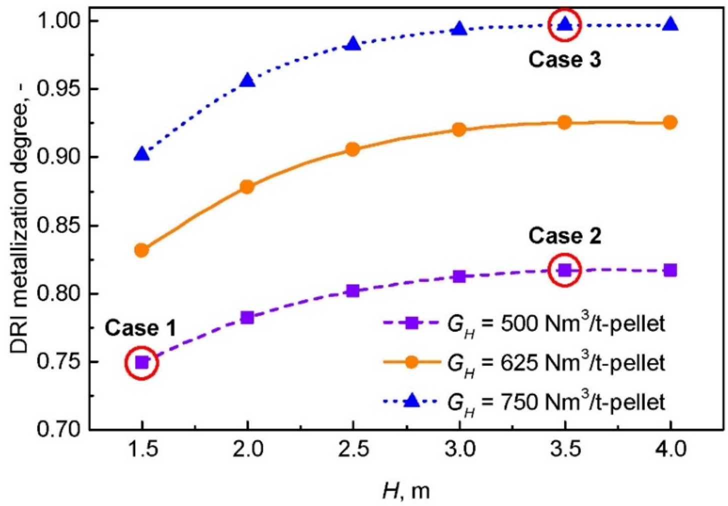

Figure 4. Effect of upper-row injection distance (H) on DRI metallization degree at different injection rates (G_H).

More interestingly, Figures 3 and 4 show that increasing the distance of the upper injection level from the top, H, can also improve the two key performance indices, although the extent is lesser. This is chiefly attributed to the fact that a longer zone facilitates a more efficient heat exchange between the ascending high-temperature injection gas and the descending solids. However, for a given G_H, the two indices are observed to grow only marginally for $H > 3.5$ m. Thus, the condition $H \approx 3.5$ m corresponds to a close-to-limit gas–solid exchange. Since a deeper injection point also leads to a higher pressure drop of the gas, the total energy demand increases because more energy is required to compress the gas. Therefore, $H = 3.5$ m is taken as a proper position of the upper-row injection under the operating conditions considered in this work.

In order to substantiate the above arguments, the distributions of burden temperature (Figure 5a) and mass fraction of metallic iron (Fe) in the burden (Figure 5b) under the conditions of Cases 1–2 (cf. Figure 4) are compared in Figure 5a, showing that the burden temperature is increased in the lower parts of the shaft as upper-row injection is shifted downward from $H = 1.5$ m (Case 1) to $H = 3.5$ m (Case 2). This is obviously beneficial for the endothermic reduction reaction and thus results in a higher DRI metallization degree, i.e., an increased mass fraction of Fe in the solid for Case 2, as depicted in Figure 5b. Moreover, the results indicate that a high microwave heating efficiency is expected in the region above H = 3.5 m, where only a little Fe, reflecting the microwaves, is present in the burden. This justifies the arrangement depicted in Figure 1, where the microwave heater is positioned above the upper-row injection level.

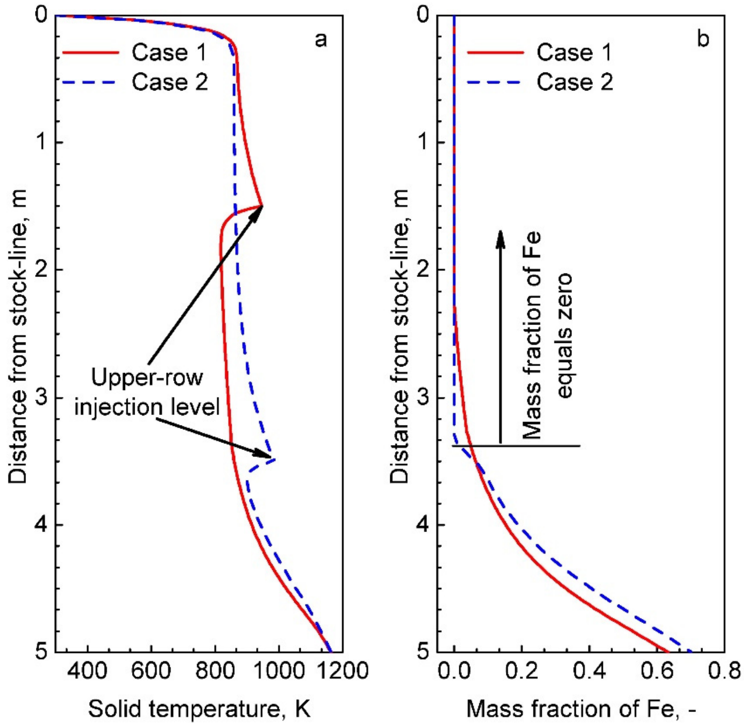

Figure 5. Distributions of solid temperature (**a**) and mass fraction of metallic iron (Fe) in the burden (**b**) under the conditions of two representative cases.

It is worth noticing that the DRI metallization degree under the conditions of Case 2 is still only about 0.82 (cf. Figure 4), which is much lower than the target value (i.e., 0.96) suggested by Duarte [21] for the H_2-based steelmaking chain in terms of overall CO_2 emissions. However, the metallization degree can be raised to almost unity by increasing G_H to 750 Nm^3/t-pellet, as seen in Case 3 of Figure 4.

3.2. Potential of Microwave Heating

Simulations were conducted for scenarios where the H_2-SF is equipped with a combination of the dual-row injection TGR system and the microwave heater to assess the potential of microwave heating to improve the performance of the unit. Being a preliminary study, only the effects of microwave power (E_{mw}) are investigated here, while sensitivity analyses of more factors will be left for future studies. The microwave heating height was chosen as U = 2.0 m and the remaining modeling parameters are identical to the ones used in Case 2.

From a theoretical point of view, heating the burden by using microwaves facilitates the endothermic process of iron oxide reduction with H_2. Figure 6 illustrates the effects of microwave heating on the distributions of burden temperature (Figure 6a) and reduction degree (Figure 6b). In comparison with Case 2, the simulation referred to as Case 4 in the figure corresponds to a scenario with E_{mw} = 1.4 MW. It is observed that the use of microwave heating gives rise to a general increase in both burden temperature and reduction degree, thus confirming the positive effect of microwave heating on the performance of the furnace. However, in evaluating the results, one should keep in mind the limitations imposed by the one-dimensional approach used in the present study.

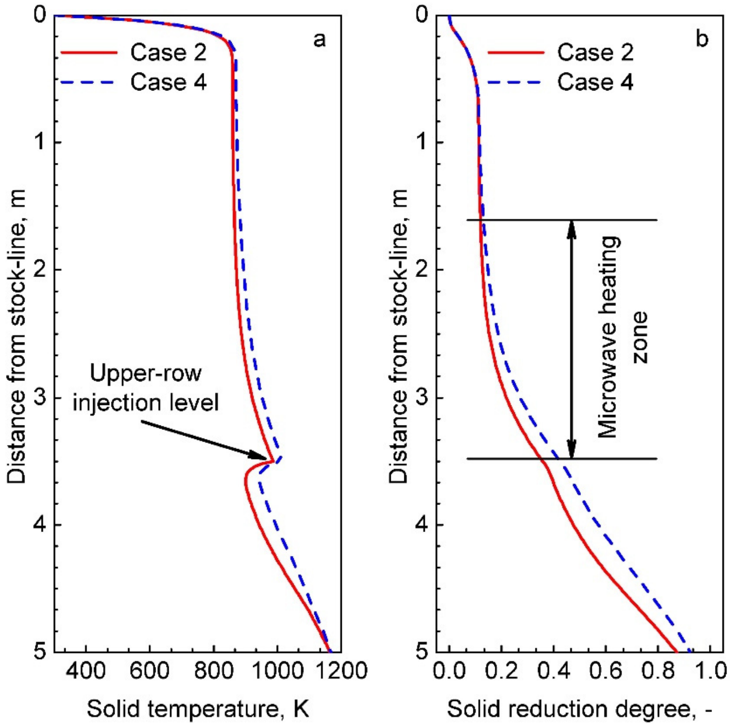

Figure 6. Effects of microwave heating (with E_{mw} = 1.4 MW) on the distributions of solid temperature (**a**) and solid reduction degree (**b**).

More simulations were carried out to study the effects of microwave power (E_{mw}). Figure 7 depicts how the top gas temperature (a), top gas utilization degree (b), DRI metallization degree (c) and furnace productivity per unit volume of reduction zone (d) vary with E_{mw}. All four performance indices are seen to improve with an increase in E_{mw} because more thermal energy can be absorbed by the solid phase, which is in turn beneficial for the process. It should be pointed out that for the simulation with E_{mw} = 4.2 MW, here referred to as Case 5, the productivity (32.4 t-Fe/(d·m^3)) is nearly identical to that of Case 3 (with a 250 Nm^3/t-pellet increase in G_H). However, the increase in G_H requires a higher heating energy, about 6.8 MW, which indicates the promising energy-saving potential by using microwave heating.

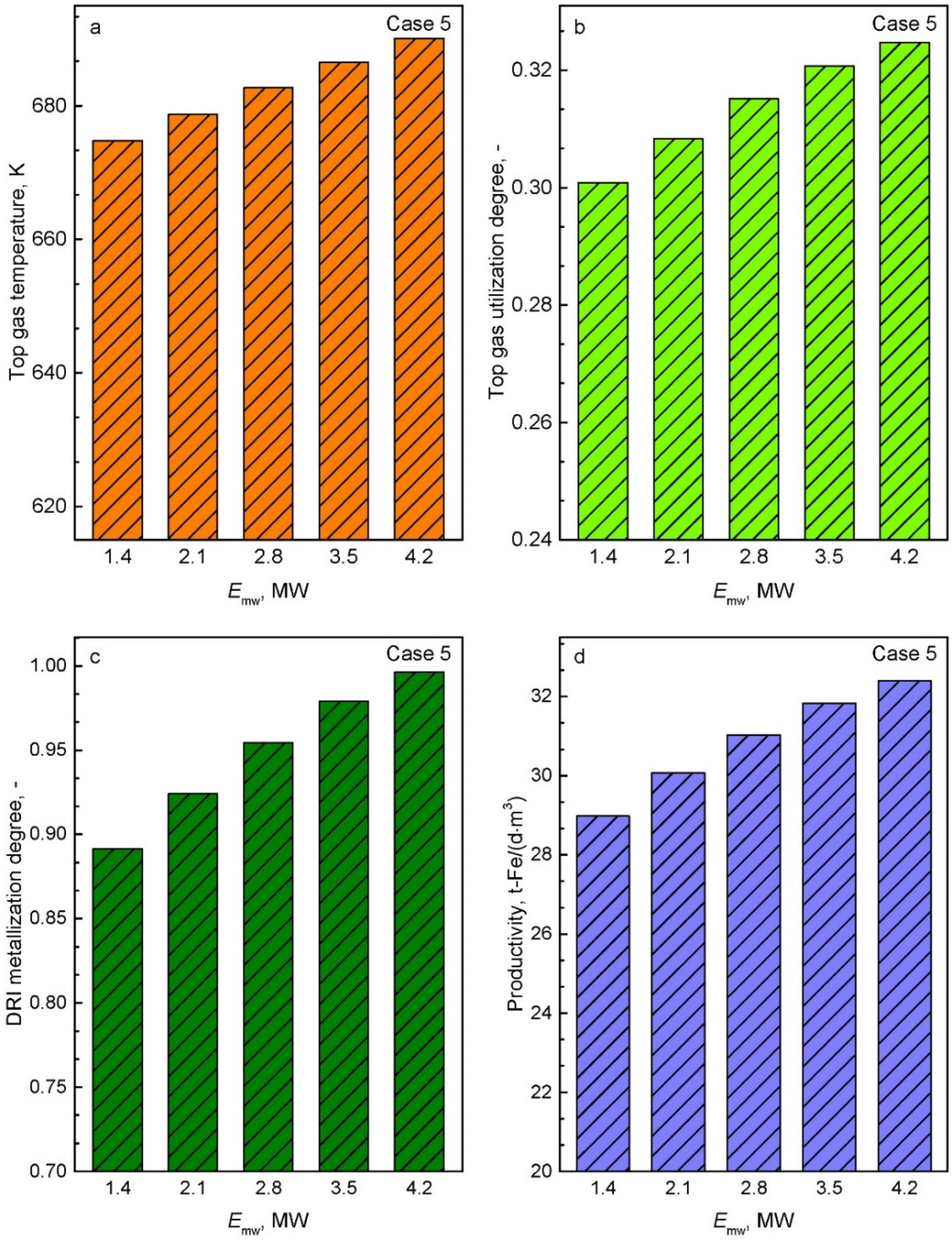

Figure 7. Effects of microwave heating power ($E_{\rm mw}$) on predicted performance indices: top gas temperature (**a**), top gas utilization degree (**b**), DRI metallization degree (**c**) and productivity (**d**).

The thermochemical state in the furnace for the scenario of Case 5 can be studied in Figure 8, where the H_2 mole fraction of the gas phase (dash-double dotted line) and the equilibrium values of each reduction step calculated based on the solid temperature are plotted. As can be seen, the mole fraction of H_2 in the gas phase decreases as the stock-line is approached, while the equilibrium fractions increase. The differences between the curve for the mole fraction of H_2 in the gas phase and the curves for the equilibrium mole fractions represent the driving forces of the reduction reaction steps. It is seen that the wustite (Fe_xO) reduction reaction, which is thermodynamically the most difficult step, takes place in the lower two thirds of the bed ($H > 1.6$ m), and its driving force increases as the lower-row injection point is approached.

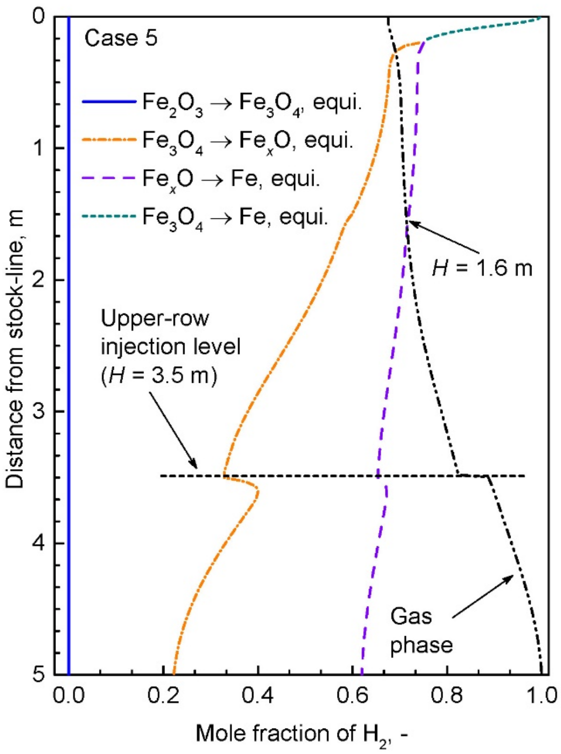

Figure 8. Comparisons between mole fraction of H_2 remaining in the gas phase and the equilibrium values of each reduction step for the scenario of Case 5.

In order to shed more light on the conditions of Case 3 and Case 5, some indices of practical interest are listed in Table 4, where the top gas temperature for Case 5 is seen to be lower than the one for Case 3. This implies that Case 5 has a better utilization of thermal energy and thus a lower energy demand. The last row of Table 4 shows that the total (specific) energy demand for Case 5 is reduced by 0.2 GJ/t-Fe compared to the one for Case 3. Assuming that the price of electricity is 100 EUR/MWh, this energy saving corresponds to a reduction of 5.6 EUR/t-Fe in the production cost for the H_2-based steelmaking chain essentially running on electricity. Moreover, the energy saving is equivalent to a decrease of 6.8 kg-coal/t-Fe in the fuel rate for the conventional coal-based steelmaking route, assuming the heating value of standard coal is 29.3 MJ/kg.

Table 4. Predicted performance indices of two cases studied in this work.

Index	Case 3	Case 5
Top gas temperature, K	718	690
Electrolysis energy, GJ/t-Fe	10.6	10.6
Heating energy, GJ/t-Fe	3.6	3.4
Compression energy, GJ/t-Fe	0.6	0.4
Microwave power, GJ/t-Fe	0	0.2
Total energy demand, GJ/t-Fe	14.8	14.6

4. Conclusions and Future Prospects

In this study, a mathematical model based on a description of the complex gas–solid countercurrent reactive flow was applied to investigate the performance of a shaft furnace for hydrogen reduction of iron oxide pellets under operation with a dual-row injection top gas recycling system. In addition, the potential of microwave heating was assessed briefly. The main findings of the study can be summarized as:

1. For scenarios without microwave heating, increasing the upper-row injection rate can improve the furnace performance, particularly in terms of top gas utilization

degree and metallization degree of the direct reduced iron (DRI). Increasing the distance of the upper-row injection level from the furnace top also has a positive effect. However, at a critical value (around 3.5 m from the top under the operating conditions considered), a further increase tends to be ineffective for improving the performance. Moreover, it is expected to be most beneficial to apply microwave heating in regions above the upper-row injection level, where little metallic iron, which reflects microwaves, is present in the burden.

2. For scenarios with microwave heating, a higher microwave power generally gives rise to a better furnace performance in terms of top gas temperature, top gas utilization degree, DRI metallization and furnace productivity.
3. A high furnace productivity can be achieved by increasing either the upper-row injection rate or the microwave power. However, the total energy demand of the latter operation decreases due to a better utilization of thermal energy. Based on the comparison of two representative cases, the decrease in the total energy demand is about 0.2 GJ/t-Fe.

Even though the potential of the new design combining gas injection on dual levels and microwave heating was found promising, it should be kept in mind that the present analysis was based on a number of gross simplifications that need to be verified or revised. For instance, the thermal and reduction behavior of the burden under the condition of microwave heating should be investigated thoroughly in order to describe the impact more accurately. This concerns both the absorption of the microwave (i.e., the energy source in Equation (3)) and the effect of microwave heating on the reaction kinetics. In conjunction with this, the kinetic parameters describing the reduction of a single pellet in Equation (2) should be revised in order to better reflect the conditions in the H_2-SF. Therefore, laboratory-scale experiments of the thermal and reduction behavior of iron oxide pellets under the conditions should be undertaken to develop sub-models of higher accuracy, which would improve the reliability of the predictions by the shaft model. Realizing the limitation of the one-dimensional approach taken in the present study, an extension to a three-dimensional model based on computational fluid dynamics is underway. This will make it possible to consider radial distributions of the state variables such as temperatures of the gas and solid phases, species fraction of the gas phase, reduction degree of the solid phase and possible asymmetry in the furnace. This will then make it possible to evaluate the penetration of microwaves and the gas injected at the upper row. Furthermore, a thorough study will be undertaken to assess the economic performance of the H_2-based steelmaking chain, as well as a lifecycle assessment to evaluate the sustainability of this alternative ironmaking process.

Author Contributions: Conceptualization, Z.Z. and H.S.; literature review, S.Y., L.S. and H.S.; original draft preparation, S.Y. and L.S.; writing—review and editing, S.Y., L.S., Z.Z. and H.S.; funding acquisition, H.S. All authors have read and agreed to the published version of the manuscript.

Funding: This research was partially funded by Business Finland and companies in the project Towards Fossil-free Steel. The authors wish to express their gratitude for the financial support.

Conflicts of Interest: The authors declare no conflict of interest. The funders had no role in the design of the study or interpretation of the results.

References

1. Pei, M.; Petäjäniemi, M.; Regnell, A.; Wijk, O. Toward a fossil free future with HYBRIT: Development of iron and steelmaking technology in Sweden and Finland. *Metals* **2020**, *10*, 972. [CrossRef]
2. Flores-Granobles, M.; Saeys, M. Minimizing CO_2 emissions with renewable energy: A comparative study of emerging technologies in the steel industry. *Energ. Environ. Sci.* **2020**, *13*, 1923–1932. [CrossRef]
3. Holappa, L. A general vision for reduction of energy consumption and CO_2 emissions from the steel industry. *Metals* **2020**, *10*, 1117. [CrossRef]
4. Patisson, F.; Mirgaux, O. Hydrogen ironmaking: How it works. *Metals* **2020**, *10*, 922. [CrossRef]
5. IEA. Available online: https://www.iea.org/reports/the-future-of-hydrogen (accessed on 15 October 2021).

6. HYBRIT. Available online: https://www.hybritdevelopment.se (accessed on 15 October 2021).
7. SALCOS. Available online: https://salcos.salzgitter-ag.com/en/mydral.html (accessed on 15 October 2021).
8. Vogl, V.; Åhman, M.; Nilsson, L.J. Assessment of hydrogen direct reduction for fossil-free steelmaking. *J. Cleaner Prod.* **2018**, *203*, 736–745. [CrossRef]
9. da Costa, A.R.; Wagner, D.; Patisson, F. Modelling a new, low CO_2 emissions, hydrogen steelmaking process. *J. Cleaner Prod.* **2013**, *46*, 27–35. [CrossRef]
10. Shao, L.; Wang, Q.; Qu, Y.; Saxén, H.; Zou, Z. A numerical study on the operation of the H_2 shaft furnace with top gas recycling. *Metall. Trans. B* **2021**, *52B*, 451–459. [CrossRef]
11. Shao, L.; Zhang, X.; Zhao, C.; Qu, Y.; Saxén, H.; Zou, Z. Computational analysis of hydrogen reduction of iron oxide pellets in a shaft furnace process. *Renew. Energ.* **2021**, *179*, 1537–1547. [CrossRef]
12. Agrawal, S.; Dhawan, N. Microwave carbothermic reduction of low-grade iron ore. *Metall. Trans. B* **2020**, *51*, 451–459. [CrossRef]
13. Colombini, E.; Papalia, K.; Barozzi, S.; Perugi, F. A novel microwave and induction heating applicator for metal making: Design and testing. *Metals* **2020**, *10*, 1576–1586. [CrossRef]
14. Hara, Y.; Sakawa, M.; Kondo, S. Mathematical model of the shaft furnace for reduction of iron-ore pellet. *Tetsu-to-Hagane* **1976**, *62*, 315–323. [CrossRef]
15. Karwa, R. *Heat and Mass Transfer*, 1st ed.; Springer Science + Business Media: Singapore, 2017; pp. 887–895.
16. Takahashi, R.; Takahashi, Y.; Yagi, J.; Omori, Y. Operation and simulation of pressurized shaft furnace for direct reduction. *Trans. Iron Steel Inst. Jpn.* **1986**, *26*, 765–774. [CrossRef]
17. Kaneko, D.; Takenaka, Y.; Kimura, Y.; Narita, K. Production of reduced iron by model plant of shaft furnace. *Trans. Iron Steel Inst. Jpn.* **1982**, *22*, 88–97. [CrossRef]
18. Takenaka, Y.; Kimura, Y. Mathematical model of direct reduction shaft furnace and its application to actual operations of a model plant. *Comput. Chem. Eng.* **1986**, *10*, 67–75. [CrossRef]
19. Parisi, D.R.; Laborde, M.A. Modeling of counter current moving bed gas-solid reactor used in direct reduction of iron ore. *Chem. Eng. J.* **2004**, *104*, 35–43. [CrossRef]
20. Shams, A.; Moazeni, F. Modeling and simulation of the MIDREX shaft furnace: Reduction, transition and cooling zones. *JOM* **2015**, *67*, 2681–2689. [CrossRef]
21. Duarte, P. Trends in hydrogen steelmaking. *Steel Times Int.* **2020**, *44*, 35–39.